We are IntechOpen, the world's leading publisher of Open Access books Built by scientists, for scientists

4,800
Open access books available

122,000
International authors and editors

135M
Downloads

Our authors are among the

154
Countries delivered to

TOP 1%
most cited scientists

12.2%
Contributors from top 500 universities

CLARIVATE ANALYTICS BOOK CITATION INDEX INDEXED

WEB OF SCIENCE™

Selection of our books indexed in the Book Citation Index in Web of Science™ Core Collection (BKCI)

Interested in publishing with us?
Contact book.department@intechopen.com

Numbers displayed above are based on latest data collected.
For more information visit www.intechopen.com

18

Multiwavelength Polarimetric Lidar for Foliage Obscured Man-Made Target Detection

Songxin Tan[1] and Jason Stoker[2]
[1]South Dakota State University
[2]USGS Earth Resources Observation and Science (EROS)
USA

1. Introduction

LIDAR is an acronym for LIght Detection And Ranging. It is also called optical radar, laser radar or ladar under different application scenarios. The fundamental principle of lidar is similar to that of the microwave radar. However, lidar operates in optical frequency while radar works in microwave frequency. There are many unique ways that light interacts with matter, hence lidar differs in many respects from radar. The interaction between light and matter has different physical mechanisms, which include Rayleigh scattering, Mie scattering, Raman scattering, resonance scattering, fluorescence, absorption, and differential absorption and scattering, etc. (Measures, 1992). The interaction is detected by lidar, and the information is used to obtain the target characteristics. Lidar can be used to characterize a wide variety of targets, from a hard target such as a vehicle or a tree, to a pure phase object such as the atmosphere or the cloud. It has been used in many remote sensing applications, including vegetation and forest monitoring, land-use and land-cover detection, land management, cloud and aerosol detection, sea shore bathymetry, global ice sheet monitoring, among many others. The information provided by lidar improves our understanding of the environment, the ecological system, and the biocomplexity of the planet Earth.

A typical lidar system consists of a laser source, transmitting optics and receiving optics, photodetector, analog–to-digital (A/D) converter, signal and data processor, and output device. A block diagram of a lidar system is illustrated in Figure 1. The sequence of lidar operation is described as follows. The laser beam is sent out through the transmitter towards the target, and the transmitted light interacts with the media and is reflected/scattered back toward the receiving optics. The photodetector then converts the received light signal into an analog electrical signal, which is further transformed into a digital signal by an A/D converter. The signal is analyzed by the signal and data processor, and the final result is sent to an output device for display.

While most existing commercial lidar systems employ one single laser wavelength and lack the polarimetric measurement capability, a new type of lidar, the multiwavelength polarimetric lidar, was introduced in vegetation remote sensing (Tan & Narayanan, 2004). The multiwavelength lidar is able to provide more spectral information about the target

under study. For example, it is well known that both coniferous and deciduous trees have similar reflectivity in visible wavelengths, but deciduous trees have distinctively higher reflectivity at near-infrared compared to coniferous trees. As a result, such spectral information at several laser wavelengths can be used for tree species classification (Jaaskelainen et al., 1994). On the other hand, polarimetric lidar provides polarization state of the backscattered laser which contains information such as target composition, surface roughness, water content, etc. The information is essential in order to understand the target characteristics. For example, a previous study found that deciduous trees had distinct depolarization signature at 1064-nm while coniferous trees had such signature at 532-nm (Kalshoven & Dabley, 1993). At this time, the understanding of polarimetric scattering property of vegetation at optical wavelengths is very limited. Both theoretical and experimental studies (Ma et al., 1990) are needed in order to fill the gap. As a new concept lidar sensor, the potential of multiwavelength polarimetric lidar is yet to be explored.

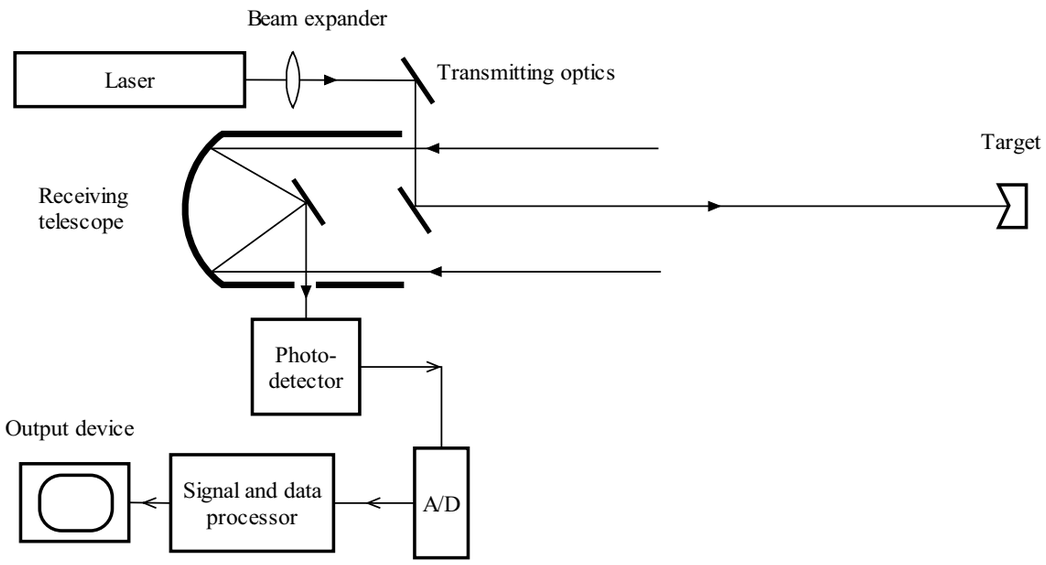

Fig. 1. Illustration of a typical lidar system.

2. Foliage Obscured Target Detection

Many remote sensing applications demand for the foliage obscured man-made objects detection. These applications may range from civilian applications, such as search and rescue missions in densely forested areas, to military applications, such as detecting camouflaged enemy vehicles. Traditional passive remote sensing has very limited capability in foliage obscured target detection. Active sensors such as the foliage penetration (FOPEN) radar has been proven successful in many applications and has become the primary tool when foliage obscured target detection is needed. Studies on foliage obscured target detection using radar technology have been reported in the literature (Nashashibi & Ulaby, 2005; Xu & Narayanan, 2003). The reason is that microwave has longer wavelength and can penetrate the vegetation canopy. The penetration ability of microwave or lightwave is related to its wavelength. Generally speaking, the longer the wavelength, the better it

penetrates. Lidar is not traditionally considered when discussing foliage penetration (FOPEN) applications. This is due to the fact that the laser wavelength is much shorter than the microwave wavelength. Therefore, a laser beam is considered as incapable of penetrating through the vegetation canopy. However, multiwavelength polarimetric lidar can be a viable alternative even though it has received little attention.

Nevertheless, gaps do naturally occur inside a forest. These include the gaps inside a single tree crown and gaps in between different tree canopies. Consequently, the target is usually not 100% covered by the foliage. If the laser beam or even a portion of the laser beam is able to go through the gaps and hit the target and return to the detector, then it is still possible to detect the hidden target using a lidar sensor. For example, a previous study demonstrated that a scanning lidar system could be used to detect the hard obstacles on the ground which were non-drivable and the foliage area which was drivable for a robotic vehicle (Castano & Matthies, 2003). It demonstrated that lidar does have certain foliage penetration capability. With its inherent shorter wavelength, lidar provides better range resolution and better spectral purity in comparison with radar. Therefore, it can offer advantage in certain target detection and identification applications.

In this study, a multiwavelength polarimetric lidar was used to detect a man-made target obscured by trees. The multiwavelength polarimetric lidar provides several advantages in target detection. Firstly, the spectral reflectance of a man-made target is usually different from that of the foliage. Even when certain type of camouflage cover or paint is applied, it is extremely difficult to match the natural foliage reflectance pattern at several different wavelengths. Secondly, the polarimetric scattering properties of the man-made target and the foliage are generally quite different. Since the polarimetric scattering property at an optical wavelength is determined by many factors such as the material composition, target shape, surface roughness, etc., it is extremely difficult to produce a camouflage that has the same polarimetric scattering feature as the foliage. Therefore, the detection rate and identification success can be improved using the combined information from spectral and polarimetric features.

3. Lidar System Description

3.1 MAPL lidar system

The lidar system built and used in this study is the Multiwavelength Airborne Polarimetric Lidar (MAPL) system. The MAPL is composed of several sub-systems: the laser source, the optical receiver assembly and the data acquisition and processing hardware and software. The MAPL system block diagram is shown in Figure 2.

The MAPL system functions as follows. A computer controls a digital delay/pulse generator through an RS-232 interface. TTL signals are then generated by the delay generator. One TTL signal is sent to trigger the Q-switch of the laser; the other TTL signal is delayed and sent to trigger the digitizer. The delay time is determined by the range of the target. The laser simultaneously sends out two laser pulses at 1064-nm and 532-nm. On top of the laser head, there is a silicon PIN detector attached to monitor the relative laser output. The laser pulses are backscattered by the target, and received by four photomultiplier tube (PMT) detectors. These detectors enable detection at both co-polarized and cross-polarized direction at the two wavelengths. Outputs from the PMT detectors are digitized by a high-speed analog to digital (A/D) converter and then sent to the computer through a PCI

interface card. The ranging ability is achieved by precisely timing the transmission and reception of the laser pulse. Data are stored in a hard drive and post-processed by the computer to extract information.

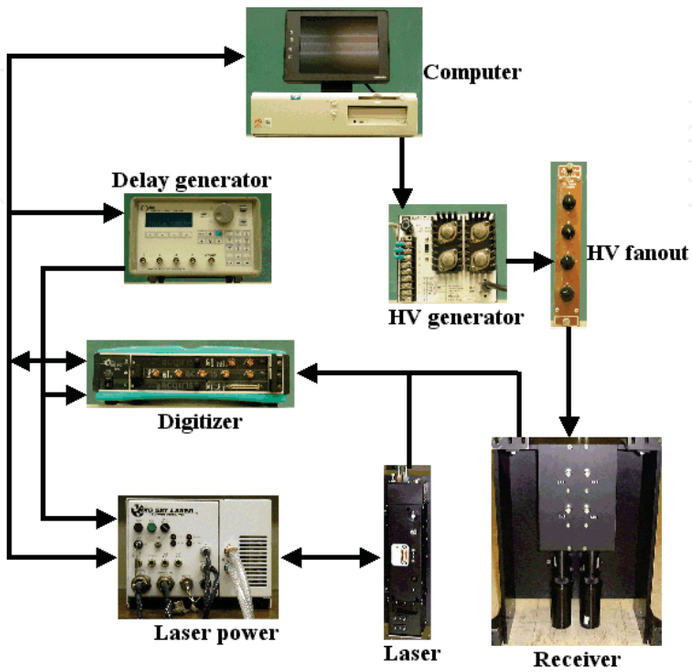

Fig. 2 Block Diagram of the MAPL system.

3.1.1 Laser

The MAPL employs a Big Sky CFR-400 Nd:YAG laser. This is a multiwavelength pulsed laser system, and is designed to be compact, rigid and stable, and is thus suitable for field applications. The laser has two outputs, one at 1064-nm and one at 532-nm, emitting from two separate apertures. Special optical wedge assembly is provided inside the laser module to ensure that the two beams are parallel. The two beams are linearly polarized in the horizontal direction. The polarization purity is greater than 100:1 at both wavelengths. Each beam has a divergence angle of about 4 mrad, which will form a laser footprint with a diameter of about 4 m at a distance of 1000 m. The highest pulse repetition rate is 10 Hz. The laser output energy is adjustable and typically 30 mJ/pulse at each wavelength is used. An attenuator can also be mounted in front of the laser head to decrease the laser output energy for safety considerations. The near field beam diameter is about 6 mm at each wavelength. The pulse width is 10 ns, which yields a range resolution of 1.5 m. To ensure accurate timing, trigger of flash lamp and Q-switch are separately controllable.

A Si PIN detector from Thorlabs is sealed using an O-ring and attached externally on top of the laser head, and is used to monitor the relative output laser energy. This serves as a reference in order to calibrate the received laser return. The power supply unit and cooling group unit are integrated into a Mini-ICE (integrated cooler and electronics) subsystem. It is a compact and rugged sub-system designed to operate in a harsh outdoor environment. A

remote control box is provided to run all the controls on the laser. An RS-232 interface is also provided for computer controls.

3.1.2 Receiving Optics

A total number of four receiving channels are employed in the MAPL system. There are two channels, one co-polarized and one cross-polarized, for the 1064-nm light; and the same configuration is used for the 532-nm light. Adding more receiving channels can enable the measurement of the Stokes parameters, which are used to fully describe the polarization state of the backscattered light. However, the circularly polarized light from the vegetation and the ground is very weak under linearly polarized laser illumination (Kalshoven & Dabney, 1993). Useful information is extremely difficult to retrieve from the circular polarization channel because of the low signal to noise ratio (Tan, Narayanan & Kalshoven, 2001). The other limiting factor comes from the system size limit. More receiving channels require a larger system which is impractical for field deployment. Thus, fully polarimetric ability is not currently integrated in the MAPL system.

The optical receiver apertures are 25 mm in diameter. There is a linear polarizer, an optical interference filter, and a single plano-convex lens with a focal length of 65 mm, inside each receiver, as shown in Figure 3. The received light is diffused onto the PMT detection plane, instead of imaging onto it. The advantage of the so-called straight-through structure is to minimize the reflection and refraction optics inside the receivers, thus reducing possible modifications to the polarization state of the backscattered light (Kalshoven & Dabney, 1993). The 1064-nm polarizers inside the receivers are from Corning Polarcor and the 532-nm polarizers are from Polaroid, both of them have polarization extinction ratios higher than 1,000:1. The system also uses narrowband interference filters from Andover. These filters have full-width-at-half-maximum (FWHM) bandwidths of 1 nm. The narrowband filters serve to reduce the background solar radiation. The peak transmission for 1064-nm filter is ~38%, and for 532-nm filter is ~47%. For each receiver there is a field stop at the focal plane of the lens, which defines the detector FOV to be 6 mrad, slightly larger than the laser beam divergence angle.

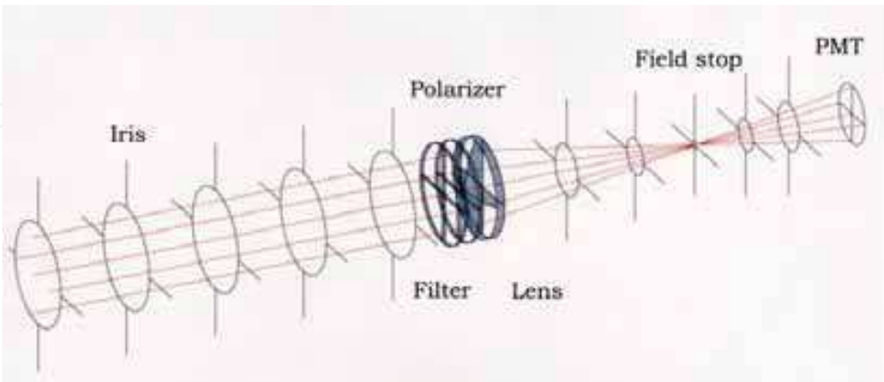

Fig. 3. The receiver optics.

Highly sensitive and ultrafast PMT detectors from Hamamatsu are used as photodetectors. Hamamatsu R632-01 is used to detect 1064-nm light, and R1464 is used for 532-nm, making good use of their spectrum response.

One important parameter for a photodetector is the minimum detectable signal. Usually this is specified by the noise equivalent power (NEP). This quantity refers to the radiant flux in watts to produce a signal to noise ratio of unity, at the output end of the detector under dark current only condition. This is also called the photon limited signal to noise ratio. In dark current limited case, the NEP is defined as (Budde, 1983)

$$NEP = \sqrt{2e \cdot i_{dark} \cdot G \cdot \Delta f} \,/\, S\,, \tag{1}$$

where S is the PMT current sensitivity at peak response wavelength, e is the electron's charge, i_{dark} is the dark current, G is the detector gain, and Δf is the bandwidth of the electronic system. At a bandwidth of 1 Hz, the NEP is 4.2×10^{-13} watts for the R632-01 detector at 1064-nm, and 1.1×10^{-15} watts for the R1464 detector at 532-nm.

From the backscattered laser signal, the cross-polarization ratio is used to quantitatively describe the polarimetric scattering property of the target surface. It is defined as the ratio between the cross-polarized return and the co-polarized return, i.e.,

$$\delta = \frac{I_{\perp}}{I_{//}}\,, \tag{2}$$

where $I_{//}$ represents the co-polarized laser return and $I_{\perp}$ represents the cross-polarized return received at the PMT detectors. The value of the cross-polarization ratio is usually within the range of 0 to 1.0. However, for some targets, it was observed that this ratio can exceed 1.0 (Kalshoven & Dabney, 1993).

3.1.3 Data Acquisition and Processing

A Berkeley Nucleonics model 555 digital delay/pulse generator is integrated in the system as a timing source. It is used to generate the control TTL signals to trigger the laser and the digitizer. The timing accuracy of the delay generator is 1 ns. For A/D conversion, two 8-bit digitizing cards, DC256 and DC110, from Acqiris are selected. The DC256 has four input channels, and a sampling rate of 500 MS/s, and is used to digitize the outputs from the PMT detectors. The DC110 has one channel, also samples at 500 MS/s, and is used to digitize the reference signal. Both cards are housed inside a modular CompactPCI crate, and connected to the computer through a PCI interface card with 100 Mb/s transfer rate. The Acqiris digitizers employ an internal time trigger interpolator with 5 ps resolution, which is used to assist timing calibration and trigger positioning. The accurate timing ability of the digitizer improves the range measurement accuracy, and helps obtain accurate lidar waveforms which record the entire history when the laser propagates and interacts with the target.

The system software is programmed using Labview. Functions of the Labview program include control of the digital delay generator, the laser, the digitizer, data recording and real time waveform display. Data are recorded and post-processed.

The photographs of the MAPL lidar system are shown in Figure 4, where the photo at the left side shows the laser head and the optical receiver assembly and the photo at the right side shows the electronic devices mounted inside a standard 19-inch rack. This is the configuration for ground experiments. The system needs to be repackaged in order to be installed inside an aircraft for future airborne missions.

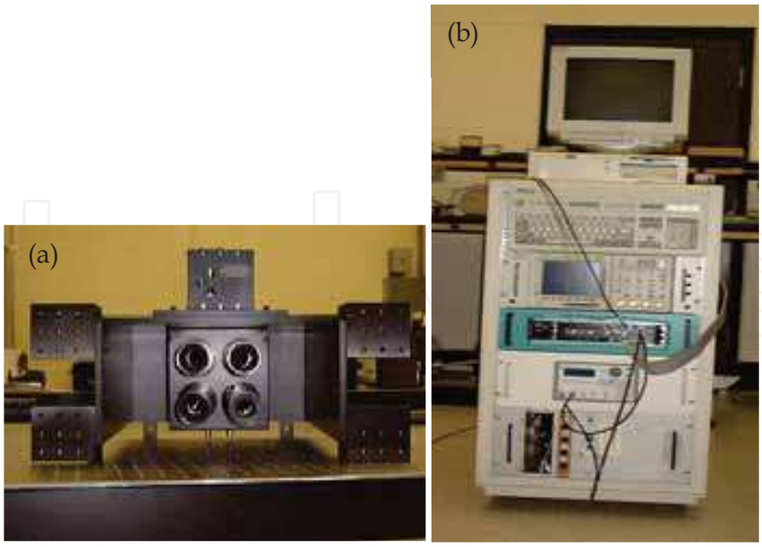

Fig. 4. Photographs of the MAPL system, where (a) is the optical assembly and (b) is the electronic subsystem.

3.2 Multiwavelength polarimetric lidar calibration

To account for the laser power output instability, photodetector gain variation and other potential error sources, the lidar data must be calibrated. Calibration is always a very difficult task. This is especially true for a polarimetric lidar where the polarimetric reflectance data calibration requires special consideration. In general, an ideal Lambertian reflection surface with known reflectivity needs to be used as a calibration standard. But an ideal Lambertian surface is extremely difficult to obtain even for laboratory measurement, not to mention the field calibration.

Measurement of materials with potential to be used as calibration standards was done inside an optical laboratory, in search of a better field calibration standard. Table 1 lists all six materials used. The Stokes parameters of these materials at both 1064-nm and 532-nm were measured to quantify their polarimetric reflectance properties. The measurement results are shown in Figure 5. We can see that the tarp and the concrete (Figure 5 (a) and (d)) resemble an ideal diffusing scatterer at both wavelengths. Their backscattered light intensities do not show strong dependence on the incident angle. Thus, it is concluded that the backscatter properties of the tarp and the concrete are close to an ideal Lambertian surface. Both of them could be used as a calibration standard in field experiments.

Canvas tarpaulin (Gosport Manufacture Inc.)
White paper (Great White® 86700)
Plywood (APA Champion 329)
Concrete (with surface polished)
Machined aluminum plate
Black anodized aluminum plate

Table 1. Materials used for Stokes parameter measurement.

In practice, the canvas tarp is used as a calibration standard due to its portability. Laboratory measurement of the polarimetric reflectance at co-polarized and cross-polarized directions from the canvas tarp is shown in Figure 6, where solid blue lines are for 1064-nm and dashed red lines are for 532-nm. The data shown here are used in the calibration for the MAPL system. The standard calibration procedure for ground experiments is described as follows. Before measuring each target, the calibration standard (i.e., the canvas tarp) is set up side-by-side with the target, and the lidar reflectance data are collected from the tarp. The high voltage supply to each PMT detector is individually adjusted to make sure that the signal has enough amplitude and is not saturated after A/D sampling. The data are compared with the laboratory measurement data as shown in Figure 6. Finally, the ratio between the averaged field calibration data and the laboratory results from the same tarp was used as a calibration constant to correct for any measurement variations. Once the calibration constant is obtained, the calibration procedure is done. Then the MAPL system is directed to the target under study and multiple measurements are recorded as raw data. These raw data from the target are then multiplied with the calibration constant to obtain the calibrated data. All future data analysis should be based on the calibrated data.

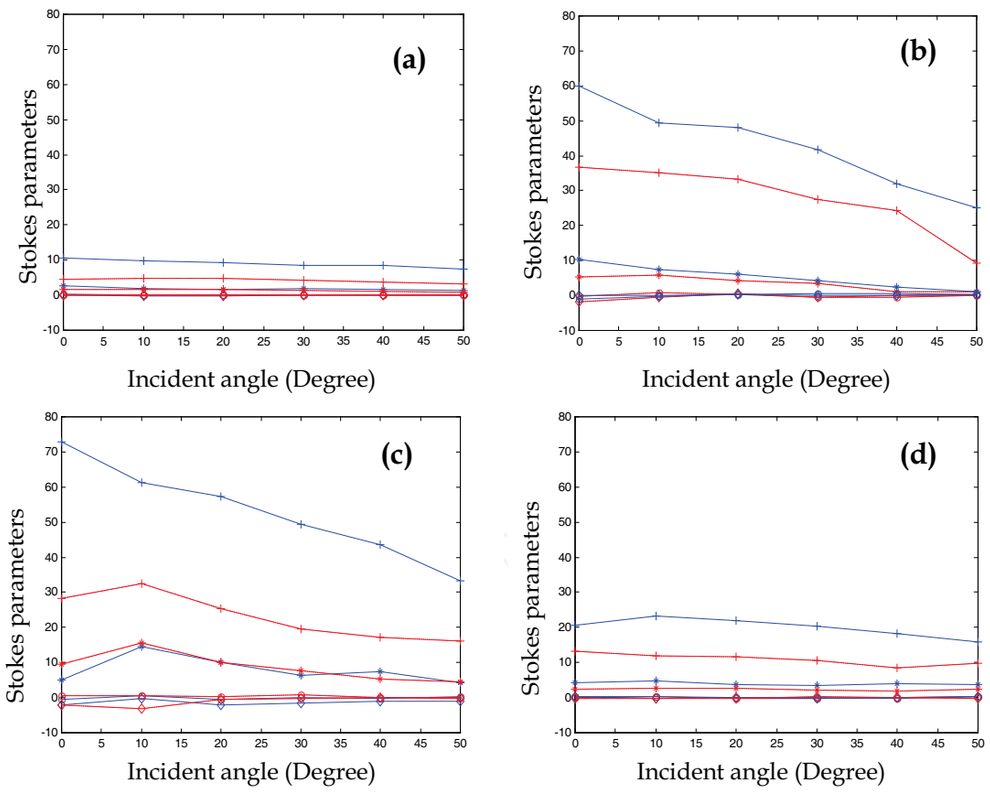

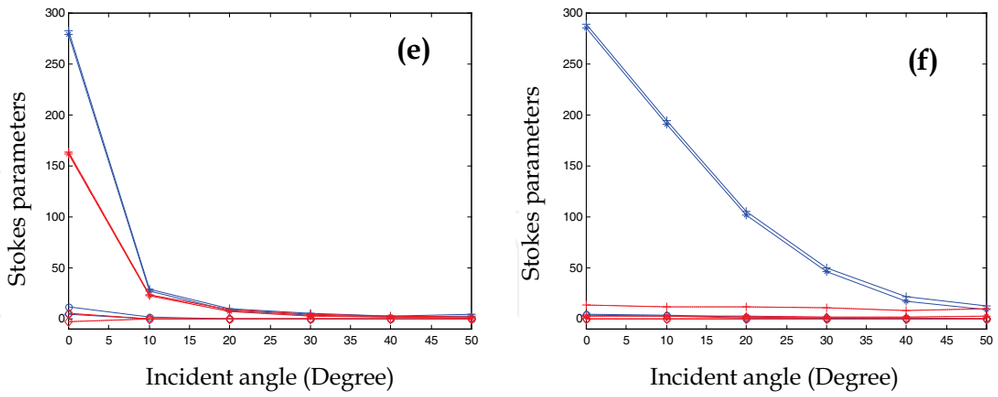

Fig. 5. Stokes parameters measurement of backscattered laser light from various materials. (a). Canvas Tarp. (b). White paper. (c). Plywood. (d). Concrete. (e). Aluminum plate. (f). Black anodized aluminum plate. ('+'=I, '*'=Q, '◊ '=U and 'o'=V. Solid blue lines are for 1064-nm and dashed red lines are for 532-nm.).

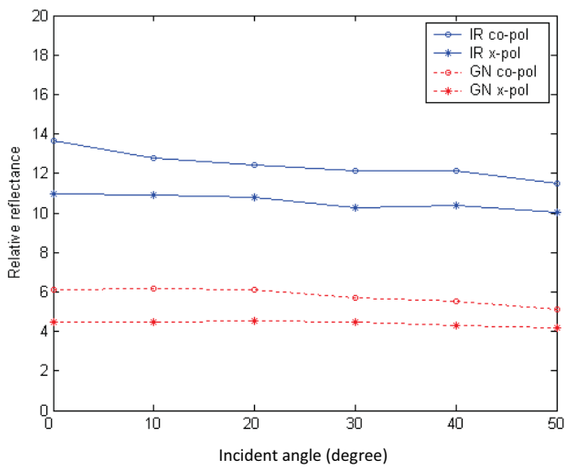

Fig. 6. Laboratory measurement of the polarimetric reflectance of a canvas at 1064-nm (solid blue lines) and 532-nm (dashed red lines) for calibration purpose.

4. Field test and data analysis

4.1 Description of the test site

The field test site was selected at Oakwood Lakes State Park in Eastern South Dakota. There were plenty of trees and shrubs inside this park. The tree species observed at the test site were primarily cottonwood, ash, oak and willow. A silver Dodge minivan was used in this experiment as a man-made target. The vehicle was parked and hidden behind several trees as shown in Figure 7. The MAPL system was set up across the lake at a distance of about 1000 m. The laser beams were shot horizontally across the lake toward the test scene.

Fig. 7. Photograph of the test site, where a vehicle was hidden inside the trees. The vehicle was ~1000 m away from the MAPL sensor. The approximate positions of the laser scans are marked by red arrows here.

The laser scanned over the test area from the left to the right. The scanning pattern is demonstrated in Figure 7. A total number of six separate scans were made during the experiment. Only one of the scans, scan number 4, coincided with the vehicle's location.

4.2 Experimental results

From the lidar data, it is observed that the vehicle paint strongly reflects near-infrared laser at both co-polarized and cross-polarized directions. The co-polarized return at 1064-nm is shown in Figure 8, where a white arrow is pointing at the vehicle position. The reflectivity of the vehicle paint at near-infrared is so strong that the returned signal is saturated after A/D conversion as seen from scan number 4. From scan lines 1, 2, 3 and 5, it is seen that the reflectance of the foliage at 1064-nm is much lower compared with the vehicle paint. The relative return of the vegetation is typically below 55 after A/D conversion. It is also observed that the top of the vegetation (scan number 1) is sparse so the returned signal strength is weaker than that at the bottom of the trees (scan number 5) where the vegetation becomes more dense. In general, it is observed that as the scan line gets lower, the returned signal becomes stronger due to more dense foliage. However, at scan number 6, the laser beam finally reaches the lake water and the returned signal becomes almost invisible. Two combined effects cause the backscattered signal level to be very low in this case. The first one is that water strongly absorbs the near-infrared laser, in comparison with foliage and vehicle paint. In addition to that, the water surface also acts as a specular surface and reflects the laser energy in the forward direction away from the detector due to the very large incident angle. As a result, there is little signal observed from scan number 6 as shown in the bottom of Figure 8. For better clarity, Figure 9 shows the image from scan number 4 separately. An arrow is used to highlight the vehicle inside the trees. All the weak scatterers in this image represent the vegetation; while the strongest reflector represents the hidden vehicle.

The direct return data from the co-polarized and cross-polarized green channels at 532-nm reveal no observable difference between the foliage and the vehicle. This is demonstrated in Figure 10 at the co-polarization channel. The result shows that the vehicle paint has a very similar reflectivity at 532-nm compared with the vegetation. Therefore, using the direct return information from a single wavelength at 532-nm and a single polarization, it is

impossible to detect the foliage-obscured vehicle. Conversely, the polarization information can provide enhanced capability in detection and identification. After computing the cross-polarization ratio following Eq. (2), the difference between the vehicle and the vegetation is revealed. The cross-polarization of the vehicle surface is significantly lower than that of the vegetation. This is partially explained by the fact that the surface of the vehicle paint is much smoother compared with the surface of vegetation leaves and barks at optical wavelength. As a result, the vehicle surface can better maintain the original linear polarization state of the incident laser thus leads to low cross-polarization ratio. Moreover, the random orientation and distribution of the tree leaves, i.e., the vegetation canopy structure, also contributes to higher depolarization during the multiple scattering process. As observed in Figure 11, the cross-polarization ratio of the vehicle (as indicated by an arrow) is typical below 0.2. On the other hand, the cross-polarization ratio of the vegetation is consistently above 0.4. At certain vegetated areas, this ratio can reach a value of larger than 0.8. This may be related to trees with very rough leaf surface and trees with very dense canopy structure.
Figure 12 and Figure 13 show the scatter plot of the returned signal at 1064-nm and 532-nm, respectively. It is clear that the classification boundary between the vegetation and the vehicle can be easily obtained in this case. From Figure 12 it is seen that the reflectivity of the vehicle paint at 1064-nm is consistently higher at both co-polarized and cross-polarized directions compared with the vegetation. The vehicle signal is so strong that it is almost always saturated. From Figure 13 it is observed that although the vehicle paint at 532-nm has comparable reflectivity in comparison with the vegetation, the cross-polarization ratio of the vehicle is much lower than that of the vegetation. The cross-polarization ratio at 1064-nm was not computed since the return data from the vehicle are saturated at both the co-polarized and cross-polarized channels. However, a logarithmic amplifier may be used in the lidar system to reduce the dynamic range of the signal. In that case, it is possible to obtain the cross-polarization ratio at 1064-nm. With the additional polarization information at 1064-nm, better detection and identification should be available for more targets.

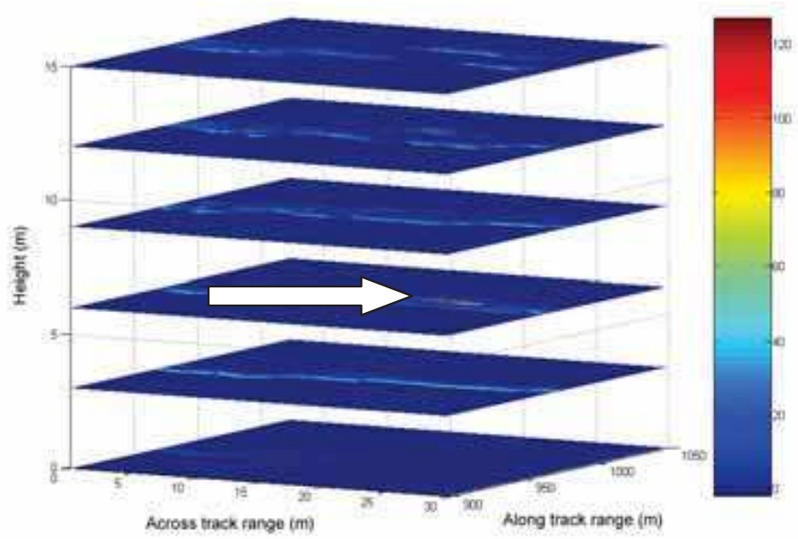

Fig. 8. Scanning result of the relative lidar return from the co-polarization channel at 1064-nm. The arrow is pointing to the vehicle inside the trees.

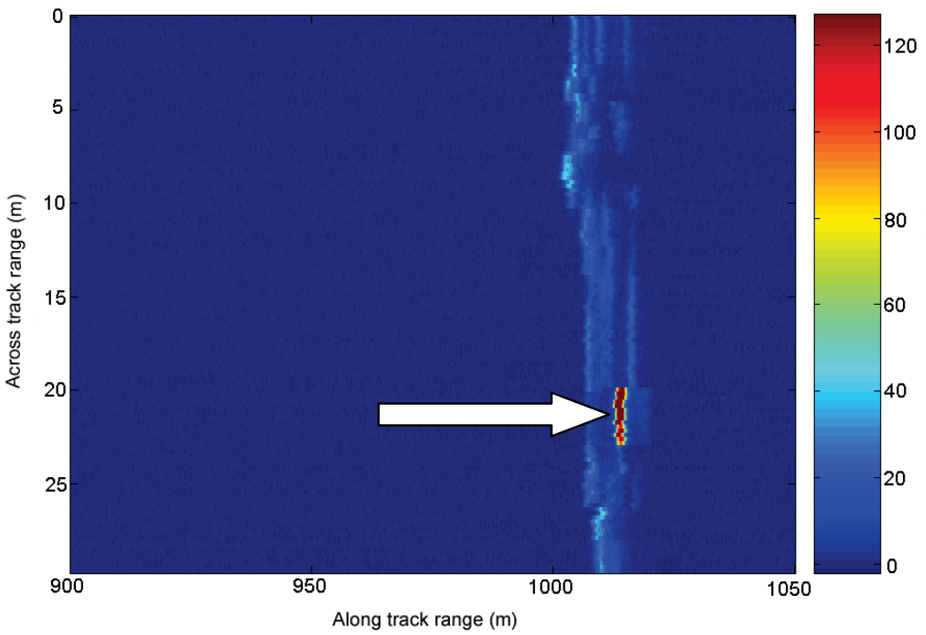

Fig. 9. Scan number 4 of the relative lidar return from 1064-nm at the co-polarization channel. The arrow is pointing to the vehicle (the strong scatterer) inside the trees (the weak scatterers).

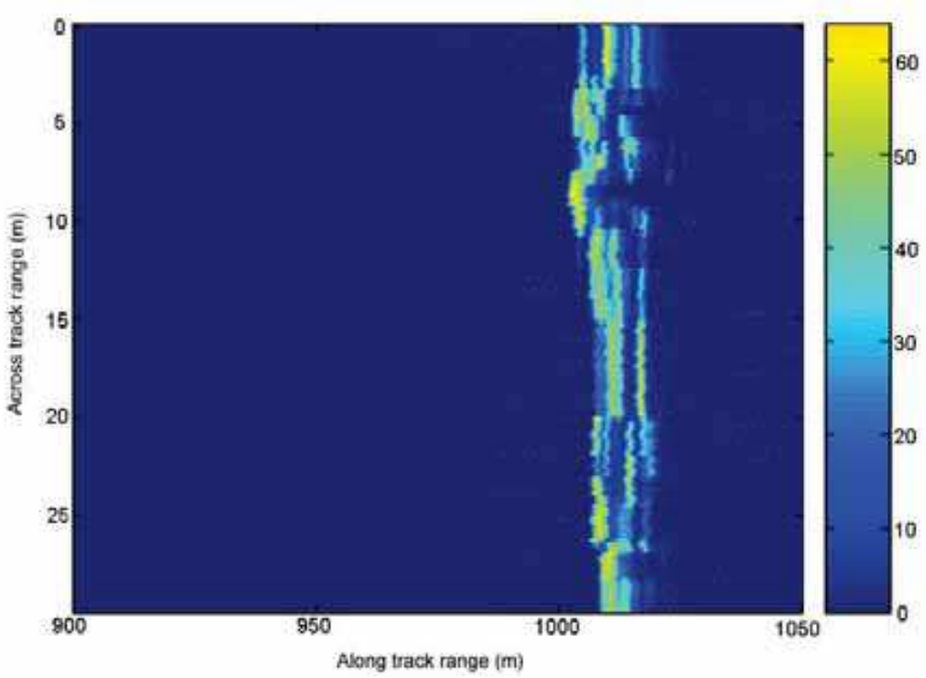

Fig. 10. Scan number 4 of the relative lidar return from 532-nm at the co-polarization channel. The vehicle could not be identified in this image.

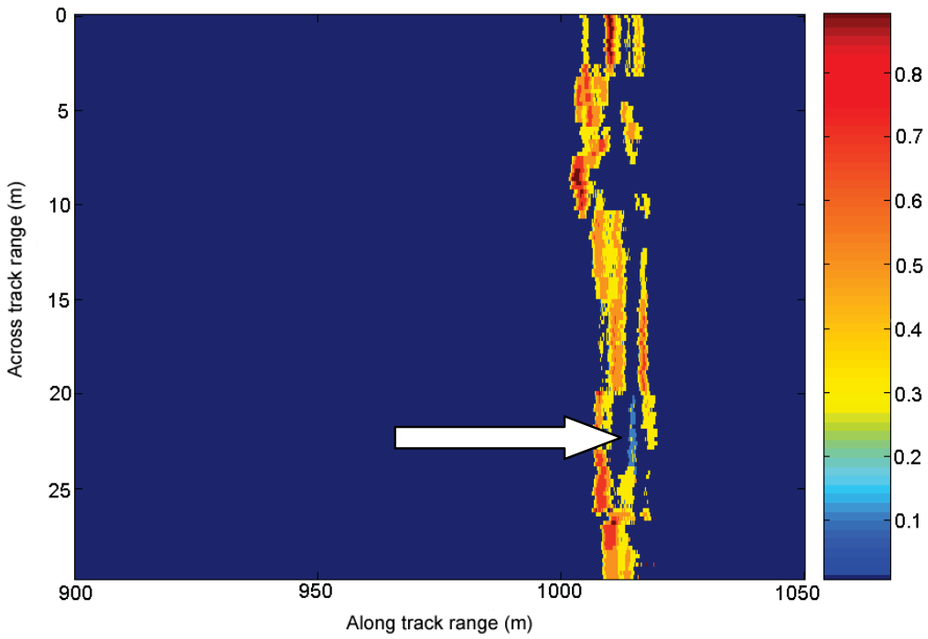

Fig. 11. The cross-polarization ratio at the 532-nm from scan number 4. The arrow is pointing to the vehicle with low cross-polarization ratio inside the trees.

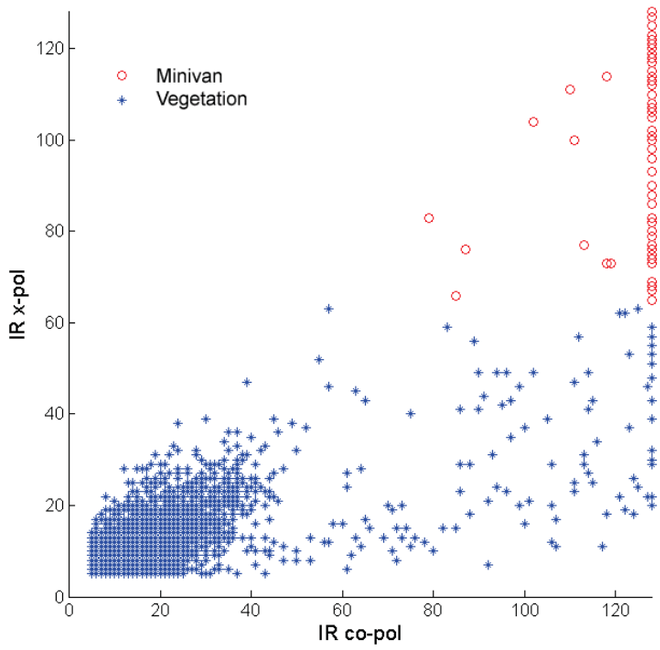

Fig. 12. Scatterplot of the lidar return at 1064-nm, where the x-axis is the co-polarization channel and the y-axis is the cross-polarization channel.

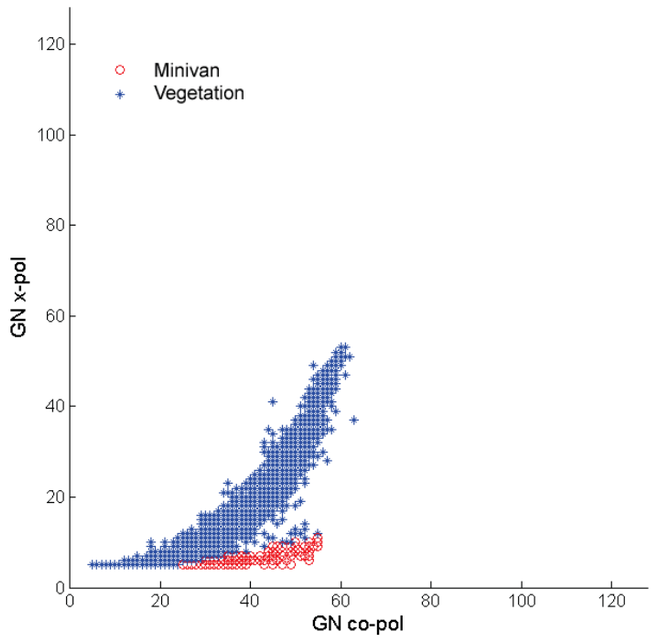

Fig. 13. Scatterplot of the lidar return at 532-nm, where the x-axis is from the co-polarization channel and the y-axis is from the cross-polarization channel.

5. Conclusions and future work

The experimental study demonstrates that the multiwavelength polarimetric lidar provides an enhanced capability in the detection of a foliage-obscured vehicle. It is revealed that the reflectivity of the vehicle and the reflectivity of the foliage are very close at 532-nm. However, at 1064-nm the reflectivity of the vehicle is significantly higher than that of the foliage. Using multiwavelength lidar in this situation demonstrates improvement in target detection. It is also shown that the cross-polarization ratio of the tree canopies is much higher than that of the vehicle at 532-nm. If a logarithmic amplifier was employed in the lidar system, the cross-polarization ratio at 1064-nm could be obtained, which can further improve the detection and identification accuracy. It is evident from the experiment that the polarimetric information provides enhanced target detection and identification capability. The multiwavelength polarimetric lidar certainly has its advantage over the existing commercial lidar systems, which are single wavelength and non-polarimetric, in target detection and identification.

In this study, only ground test data were collected. The airborne lidar data are expensive and were not collected at the time. However, it is known that more openings of the forest canopies are observed looking from above the ground. This means that the laser beam has a better chance to penetrate the tree canopies from airborne sensors. As a result, there is a better chance to detect the foliage obscured target from an airborne lidar sensor than from a ground based sensor.

This study also demonstrates the validity of the technique to detect and identify other foliage-obscured man-made targets using a multiwavelength polarimetric lidar. As long as we can find the difference in the spectral reflectance or polarimetric reflectance between the man-made target and the vegetation, we can always employ this technique. The selection of appropriate laser wavelengths and polarization combinations should be able to maximize the differences between the vegetation and the man-made target, hence enable the detection of many other types of man-made targets.

Further research is needed in order to use this multiwavelength polarimetric lidar detection technique in practical applications. From the lidar hardware side, many improvements could be made. For example, a tunable laser could be used in the system to provide a wide range of laser wavelengths for better detection. Furthermore, we can introduce a logarithm amplifier or a 12-bit (or higher) A/D converter instead of an 8-bit one in the lidar system to make sure that the system can handle signals at a larger dynamic range without signal saturation. Polarimetric lidar calibration is another challenge and better calibration strategy still needs to be explored. A polarimetric calibration standard that has a constant polarimetric reflectance property over repeated use and is easy to deploy in the field is desired. Even more importantly, efforts need to be made for the multiwavelength polarimetric lidar operation and data processing to be simple enough so that even a person with limited engineering background can operate such a sensor. From the software side, an algorithm that can automatically detect and identify the targets needs be developed. Both artificial neural networks (NN) and support vector machine (SVM) seem to be good candidates for automated data processing. The classification accuracy will be improved if we understand the target polarimetric scattering characteristics. Such understanding can greatly facilitate the development of classification algorithm. At this time, however, there is only limited research available. Consequently, more studies on the polarimetric scattering properties of both man-made targets and vegetation are in urgent need (Tan, Narayanan & Helder, 2005). In addition, more ground experiments are also needed. For example, man-made targets under camouflage conditions need to be tested. Camouflage presents a challenge in target detection. However, multiple-wavelength and polarization should provide advantage over existing lidar technology for camouflaged target detection. Camouflage is usually designed to match the spectral reflectance of the background. It is usually not intended to match the polarimetric reflectance of the background. Even if anybody wanted to do so, it would be extremely difficult to control the polarimetric reflectance of the camouflage. Therefore, a polarimetric lidar have a better chance to detect and identify the camouflaged target.

In summary, the multiwavelength polarimetric lidar is a new concept lidar in foliage obscured man-made target detection. Even though more studies are needed in this new technology, the experimental study clearly serves the purpose to demonstrate that the multiwavelength polarimetric lidar can provide better target detection and identification over the traditional single wavelength and non-polarimetric lidar system.

6. References

Budde, W. (1983). Physical detectors of optical radiation, In : *Optical Radiation Measurements*, Grum, F. & Bartleson, C. (Ed.), Academic, New York.

Castano, A. & Matthies, L. (2003). Folidage discrimination using a rotating ladar, *IEEE Internation Conference on Robotics and Automation,* Vol. 1, pp. 1-6.

Jaaskelainen, T.; Silvennoinen, R.; Hiltunen, J.; & Parkkinen, P. (1994). Classification of the reflectance spectra of pine, spruce and birch, *Applied Optics*, Vol. 33, No. 12, pp. 2356-2362.

Kalshoven, J. & Dabley, P. (1993). Remote sensing of the Earth's surface with an airborne polarimetric laser, *IEEE Trans. Geoscience and Remote Sensing*, Vol. 31, pp. 438-446.

Ma, Q.; Ishimazu, A.; Phu P.; & Kuga, Y, (1990). Transmission, reflection, and depolarization of an optical wave for a single leaf, *IEEE Trans. Geoscience and Remote Sensing*, Vol. 28, pp. 865-872.

Measures, R. (1992), *Laser Remote Sensing: Fundamentals and Applications*, Krieder Publishing, Malabar, FL.

Nashashibi, A. & Ulaby, F. (2005). Detection of stationary foliage-obscured targets by polarimetric millimeter-wave radar, *IEEE Trans. Geoscience and Remote Sensing*, Vol. 43, pp. 13-23.

Tan, S.; Narayanan, R. & Kalshoven J. (2001). Measurement of Stokes parameters of materials at 1064-nm and 532-nm wavelengths, *Proc. SPIE, laser radar technology and applications VI*, Vol. 4377, pp. 263-271.

Tan, S. & Narayanan, R. (2004). Design and performance of a multiwavelength airborne polarimertric lidar for vegetation remote sensing, *Applied Optics*, Vol. 43, pp. 2360-2368.

Tan, S.; Narayanan, R. & Helder, D. (2005). Polarimetric reflectance and depolarization ratio from several tree species using a multiwavelength polarimetric lidar, *Proc. SPIE, Polarization Science and Remote Sensing II*, Vol. 5888, 5888-23.

Xu, X. & Narayanan, R. (2003). FOPEN SAR imaging using UWB step-frequency and random noise waveforms, *IEEE Trans. Aerospace and Electronic Systems*, Vol. 37, pp. 1287-1300.

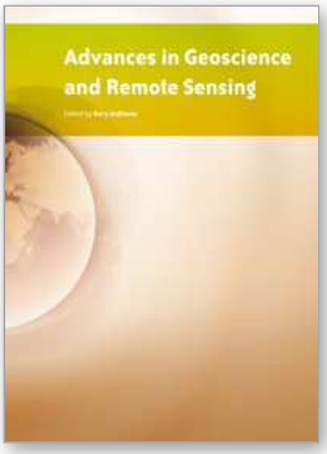

Advances in Geoscience and Remote Sensing
Edited by Gary Jedlovec

ISBN 978-953-307-005-6
Hard cover, 742 pages
Publisher InTech
Published online 01, October, 2009
Published in print edition October, 2009

Remote sensing is the acquisition of information of an object or phenomenon, by the use of either recording or real-time sensing device(s), that is not in physical or intimate contact with the object (such as by way of aircraft, spacecraft, satellite, buoy, or ship). In practice, remote sensing is the stand-off collection through the use of a variety of devices for gathering information on a given object or area. Human existence is dependent on our ability to understand, utilize, manage and maintain the environment we live in - Geoscience is the science that seeks to achieve these goals. This book is a collection of contributions from world-class scientists, engineers and educators engaged in the fields of geoscience and remote sensing.

INTECH
open science | open minds

InTech Europe
University Campus STeP Ri
Slavka Krautzeka 83/A
51000 Rijeka, Croatia
Phone: +385 (51) 770 447
Fax: +385 (51) 686 166
www.intechopen.com

InTech China
Unit 405, Office Block, Hotel Equatorial Shanghai
No.65, Yan An Road (West), Shanghai, 200040, China
中国上海市延安西路65号上海国际贵都大饭店办公楼405单元
Phone: +86-21-62489820
Fax: +86-21-62489821

IntechOpen